Journal of Medicinal Chemistry

Article

pubs.acs.org/jmc

The 1.8 Å Crystal Structure of ACTIBIND Suggests a Mode of Action for T2 Ribonucleases As Antitumorigenic Agents

Marina de Leeuw,[†] Ana González,[‡] Assaf Lanir,[†] Levava Roiz,[§] Patricia Smirnoff,[∥] Betty Schwartz,[∥] Oded Shoseyov,[§] and Orna Almog*[,†]

[†]Department of Clinical Biochemistry, Faculty of Health Sciences, Ben-Gurion University of the Negev, Beer Sheva 84105, Israel

[‡]Stanford Synchrotron Radiation Laboratory, 2575 Sand Hill Road, MS 99, Menlo Park, California 94025, United States

[§]The Institute of Plant Sciences and Genetics in Agriculture, and [∥]The Institute of Biochemistry, Food Science and Nutrition, The Faculty of Agricultural, Food and Environmental Quality Sciences, The Hebrew University of Jerusalem, P.O. Box 12, Rehovot 76100, Israel

ABSTRACT: ACTIBIND and its human homologue RNASET2 are T2 ribonucleases (RNases). RNases are ubiquitous and efficient enzymes that hydrolyze RNA to 3′ mononucleotides and also possess antitumorigenic and antiangiogenic activities. Previously, we have shown that ACTIBIND and RNASET2 bind actin and interfere with the cytoskeletal network structure, thereby inhibiting cell motility and invasiveness in cancer and in endothelial cells. We also showed that ACTIBIND binds actin in a molar ratio of 1:2. Here, we further characterize ACTIBIND and determine its crystal structure at 1.8 Å resolution, which enables us to propose two structural elements that create binding sites to actin. We suggest that each of these binding sites is composed of one cysteine residue and one conserved amino acid region. These binding sites possibly interfere with the cytoskeleton network structure and as such may be responsible for the antitumorigenic and antiangiogenic activities of ACTIBIND and its human analogue RNASET2.

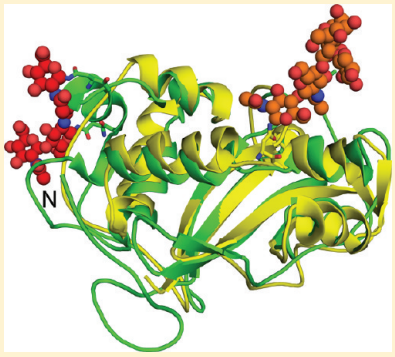

INTRODUCTION

Ribonucleases (RNases) are ubiquitous and efficient enzymes which hydrolyze RNA to 3′ mononucleotides via 2′, 3′ cyclic nucleotides. RNases have been classified into three distinct families, RNase A, T1 RNase, and T2 RNase, as based on their molar mass (11−14, 12, 20−40, respectively) and specificity toward pyrimidine bases, guanine bases, or nonspecific bases, respectively.[1] RNases display a variety of biological activities in addition to their ability to degrade RNA.[2] For example, members of the RNase T2 family from microorganisms and plants digest extracellular polyribonucleotides, thereby accelerating phosphate uptake. Other T2 RNases are involved in defense against possible pathogens.[3,4] In addition, specific T2 RNases encoded by the S locus are responsible for rejecting self-pollen, thus preventing self-fertilization.[5,6] In tomato plants, T2-RNases are induced on senescence.[7]

ACTIBIND, which is produced by the mold *Aspergillus niger* B1 (CMI CC 324626), is a member of the RNase T2 family. We have previously shown that ACTIBIND contains 32 and 36 kD isoforms, both of which share a common 29 kDa protein moiety.[8] Binding assays of ACTIBIND to actin indicated a binding ratio of 1:2.[9] We further reported that ACTIBIND binds cell surface actin,[10] which was previously shown to act as a receptor for angiogenin in endothelial cells.[11] These findings suggest that ACTIBIND interferes with the intracellar actin network structure, leading to inhibition of cell extension and migration in cancer and endothelial cells.[8,12] In mice, ACTIBIND inhibited HT-29 colon cancer and A375SM melanoma-derived xenografts as well as tumor development. In rats, ACTIBIND exerted preventive and therapeutic effects on dimethylhydrazine (DMH)-induced colonic tumors.[10,12]

Interestingly, the human RNASET2 protein, which is also a member of the T2 RNase family,[13,14] shares a considerable amino acid homology (27%) with ACTIBIND and is associated with several malignancies (e.g., ovary,[15,16] breast,[17,18] and colon/rectum[19]).

The crystal structures of several members of the T2 RNase family were previously determined, including RNase Rh (PDB entry 1bol) from the mold *Rhizopus niveus*,[20,21] RNase LE (PDB entry 1dix), from cultured cells of *Lycopersicon esculentum*,[22] RNase MC1 (PDB entry 1bk7) from *Momordica charantia* seeds,[23] S_3 RNase (PDB entry 1iqq) from *Pyrus pyrifolia*,[24] S_{F11} RNase from *Nicotiana alata* (ornamental tobacco; PDB entry 1ioo),[25] and RNase I (PDB entry 2ea1) from *Escherichia coli*.[26] A comparison of the crystal structures of these T2 RNases revealed that they belong to the $\alpha + \beta$ type class of proteins. The core of these T2 RNases includes the conserved active site which is responsible for degrading RNA. Structural differences among these T2 RNases are found mainly in their exposed surface loop regions and may be associated with their specific biological activity.

In this work, we determined the crystal structure of ACTIBIND at 1.8 Å resolution and used it to search for the

Received: December 4, 2010
Published: January 4, 2012

dx.doi.org/10.1021/jm1015507 | *J. Med. Chem.* 2012, 55, 1013−1020

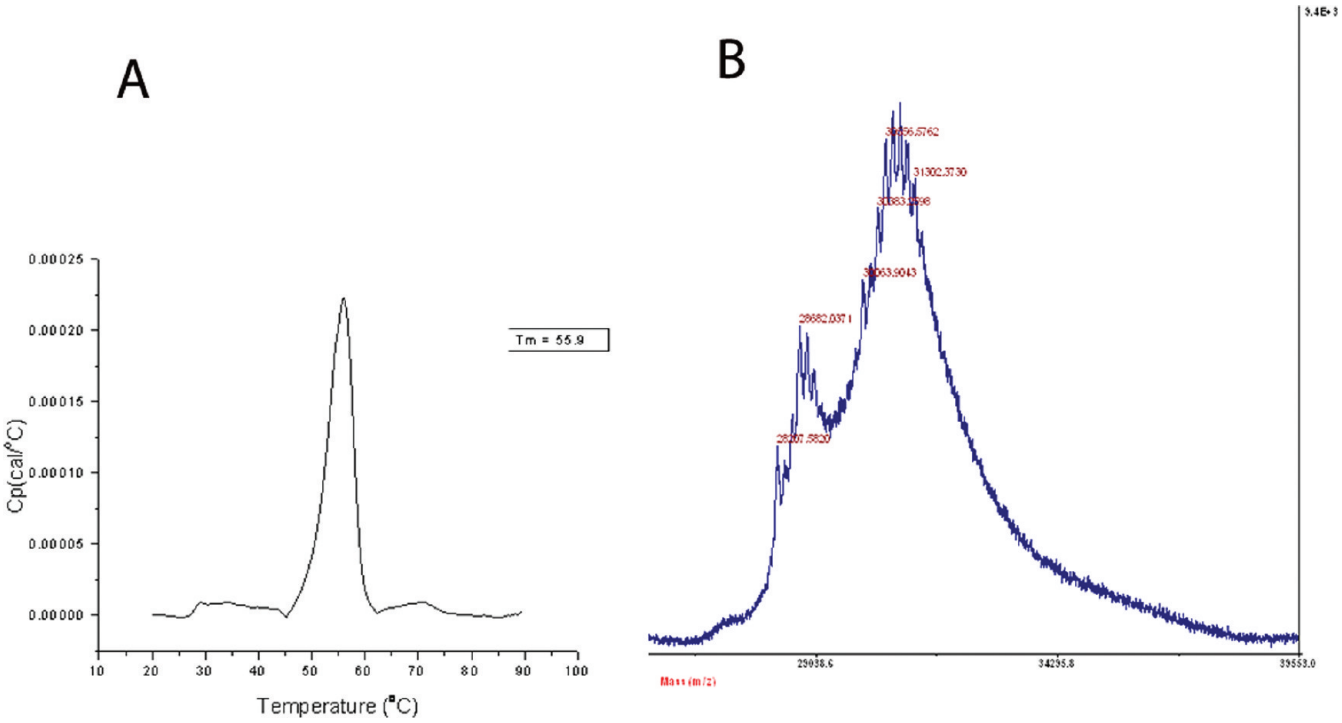

Figure 1. Biochemical characterization of ACTIBIND. (a) Differential scanning calorimetry (DSC) scan of ACTIBIND indicating a Tm of 55.9 °C. (b) MALDI-TOF analysis of ACTIBIND indicating two peaks at a molar mass of 30.56 and 28.68.

structural element that is important for its antitumorigenic activity. Previously, it was suggested that the glycosylation sites of T2 RNases, which are located on the surface of the molecules, are necessary for this activity. In contrast, our present comparison of the crystal structures of ACTIBIND and other T2 RNases revealed considerable differences in the location and the orientation of the glycan side chains, suggesting that neither the glycan sites themselves nor their location on the molecule are involved. However, we were able to locate two new structural elements common to all T2 RNases which may serve as actin binding sites, thereby inhibiting cell proliferation and tumor growth.

RESULTS

Biochemical Characterization of ACTIBIND. *ACTIBIND is a Thermostable Glycoprotein.* The differential scanning calorimetry (DSC) study of ACTIBIND showed a single peak with a T_m of 55.9 °C (Figure 1A), indicating that ACTIBIND is a thermostable protein similar to other T2-RNases.[27] Nonetheless, following extreme heat inactivation, ACTIBIND lost its RNase activity (as shown in Figure 2, lane 7) but did maintain its biological activity.

MALDI-TOF-MS experiments indicated that ACTIBIND has a major peak at a molar mass of 30558 and a smaller peak at 28682 (Figure 1B). The calculated molar mass based on the amino acids sequence is 27660. One explanation for the discrepancies in the molar mass may be that ACTIBIND has two glycosylation forms which differ by the level of glycosylation (one form with a molar mass of 30558 and the other with a molar mass of 28682). The SDS-PAGE analysis (Figure 2) revealed that ACTIBIND in solution (Figure 2, lane 2) as well as in the crystals (Figure 2, lane 3) appear as a double band at about 30000. This is in agreement with our MALDI-TOF-MS results which are shown in Figure 1B.

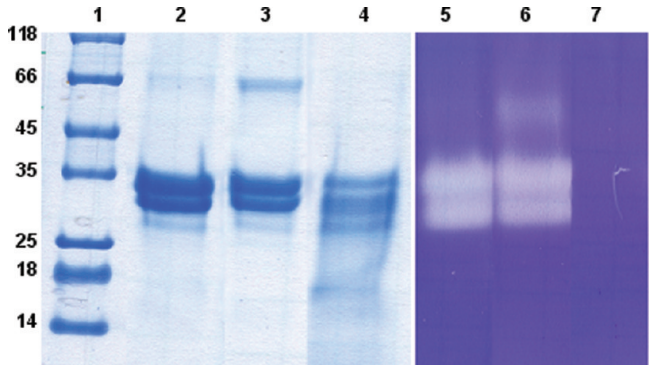

Figure 2. SDS-PAGE analysis of ACTIBIND. Lane 1, molecular markers; lanes 2–4, coomassie-blue staining of ACTIBIND in solution (lane 2), ACTIBIND in crystals (lane 3), and ACTIBIND solution after extreme heat inactivation by autoclave (lane 4). Protein samples were boiled for 10 min with denaturing application buffer. The RNase activity zymogram is shown in lanes 5–7, ACTIBIND in solution (lane 5, 10 μg/well), ACTIBIND after dissolving the crystals (lane 6; 1 crystal/well), ACTIBIND inactivated by autoclave (lane 7, 10 μg/well).

Similar to other T2 RNases ACTIBIND Possesses Biological Activity. Human umbilical vein endothelial (HUVE) cell tube formation assay on Matrigel was conducted to compare the antiangiogenic effect of ACTIBIND with that of other T2 RNases (Figure 3). Using angiogenin (Figure 3A–E) and bFGF (Figure 3F–H) as angiogenic growth factors, ACTIBIND was found to significantly inhibit both angiogenin- (Figure 3B) and bFGF-induced (Figure 3G) HUVEC tube formation. RNase MC1 (*M. charantia*) had a similar inhibitory effect on both growth factors (parts C and H of Figure 3, respectively). The inhibitory effect on tube formation of RNase T2 from *Aspergillus oryzae* (Figure 3D) and RNase I from *E. coli* (Figure 3E) was tested using only angiogenin as a growth

dx.doi.org/10.1021/jm1015507 | J. Med. Chem. 2012, 55, 1013–1020

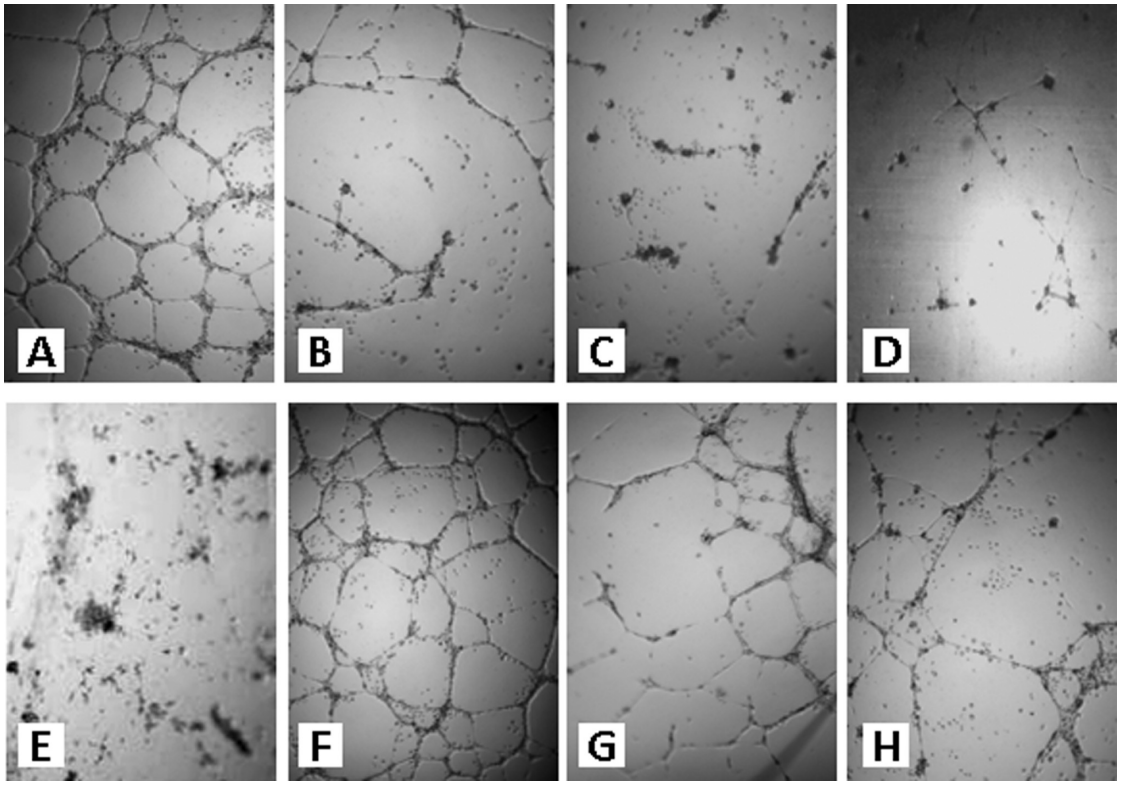

Figure 3. HUVEC tube formation on Matrigel induced by angiogenin (A–E) and bFGF (F–H). Control (A, F); 10 μM ACTIBIND (B, G); RNase MC1 (C, H); *A. oryzae* RNase T2 (D); *E. coli* RNase I (E). ACTIBIND as well as the other T2 RNases inhibit both angiogenin and bFGF-induced tube formation (N = 5 for each treatment).

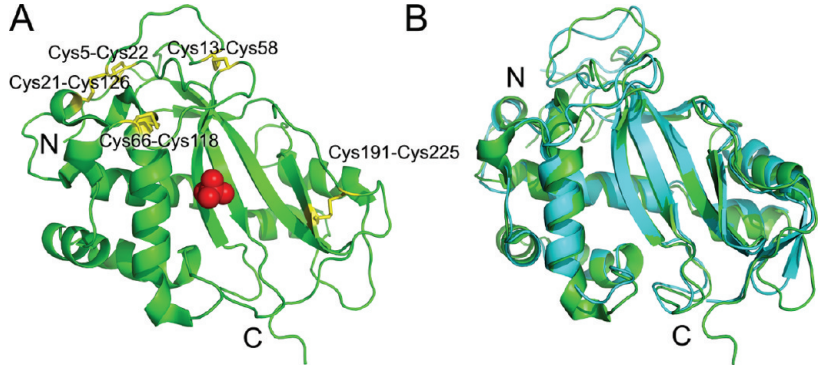

Figure 4. ACTIBIND crystal structure. (A) Final model of ACTIBIND shown as green ribbon; Cys residues are highlighted as yellow sticks; the phosphate ion at the active site region is shown as red spheres. (B) Superposition of ACTIBIND crystal structure (PDB entry 3tbz, in green) and RNase Rh (PDB entry 1bol, in blue) crystal structure.

factor. These results suggest that the biological activity of ACTIBIND as an antitumorigenic and antiangiogentic agent is common for several members of the T2 RNase family.

Structural Characterization ACTIBIND. *The Crystal Structure of ACTIBIND.* The final model of ACTIBIND consisted of 1878 protein atoms, 279 water molecules, and 71 heteroatoms (Figure 4A). The crystallographic R factor was 15.5% for the data between 33.9 and 1.8 Å resolution (R_{free} was 18.7% for 5.0% of the data). The final model was evaluated with the program package PROCHECK.[28] A summary of the data collection and refinement statistics is shown in Table 1. The Ramachandran plot indicated that 96.2% of ACTIBIND residues are in the most favored regions and 3.8% in the additional allowed regions.

Superposition of the crystal structures of ACTIBIND and that of RNase Rh (PDB entry 1bol) is shown in Figure 4B. The root-mean-square (rms) deviation between these two structures is 1.2 Å (for 205 Cαs). Major differences were found in the N-terminal region. The N-terminal region of ACTIBIND is oriented toward the solvent, whereas in the RNase Rh crystal structure, it is oriented toward the core of the molecule. Both ACTIBIND and RNase Rh belong to the structural class of $\alpha + \beta$ type protein and contain six α-helices that surround a five-β-strand core.[29] The final model of ACTIBIND includes 238 out of 247 residues. The last nine residues at the C-terminal end (SKKIYGSSL) were not included in the final model due to the lack of electron density.

The ACTIBIND crystal structure clearly indicates five disulfide bonds (Cys5–Cys22, Cys13–Cys58, Cys21–

dx.doi.org/10.1021/jm1015507 | *J. Med. Chem.* 2012, 55, 1013–1020

Table 1. Data Collection and Refinement Statistics for ACTIBIND (PDB entry 3tbz)

	overall	inner shell	outer shell
Data Collection			
low resolution limit	36.69	36.69	1.90
high resolution limit	1.80	5.70	1.80
R_{merge}	0.060	0.018	0.704
R_{meas} (within $I+/I-$)	0.067	0.021	0.789
R_{pim} (within $I+/I-$)	0.029	0.009	0.350
total no. of observations	182969	5956	23510
total no. of unique reflections	34534	1194	4913
mean((I)/sd(I))	19.0	63.7	2.0
completeness	99.7	99.0	98.6
multiplicity	5.3	5.0	4.8
unit cell	a = 78.46 Å	b = 78.46 Å	c = 103.71 Å
	α = 90.0°	β = 90.0°	γ = 120.0°
space group	$P3_221$		
solvent content (%)	64.35		
Wilson B	25.3		
Refinement			
reflections in work data set	32945		
reflections in test set	1738		
R value (working + test set)	0.155		
R value (working set)	0.154		
free R value	0.187		
protein atoms	1878		
solvent atoms	278		
phosphate ion	2		
rms Deviations from Restraints Target Value			
bond length (Å)	0.026		
bond angle (deg)	2.095		
average B factor (for protein atoms) (Å^2)	27.70		

Cys126, Cys66−Cys118, and Cys191−Cys225) as shown in Figure 4A. Interestingly, four of the disulfide bonds are located in the N-terminal region and are in proximity to each other. One disulfide bond Cys191−Cys225 is found in the C-terminal region (Figure 4A). In addition, the final model of ACTIBIND contains a phosphate ion in the active site region, near some electron density which could be interpreted as a disordered nucleotide. Three sugar molecules (*N*-acetyl-D-glucosamine, NAG) were fitted into the electron density map and are included in the final model. There is a difference of one amino acid between the ACTIBIND sequence that was previously deposited in the gene bank (GI: 71064123) and the final model. Residue 46 was fitted to the electron density as aspartate, while in the deposited sequence it was reported as glycine.

The Active Site of ACTIBIND. The ACTIBIND catalytic site which is responsible for RNA degradation is composed of residues His51, His110, His115, and Glu111 (ACTIBIND numbering) and Trp54, Asp56, and Tyr62 which are involved in binding the target base. These residues are located on the surface of the molecule, thereby creating a cavity for the substrate. A comparison of the RNA degrading sites of ACTIBIND and that of RNase Rh showed that all of the residues responsible for degradation of RNA are superimposable (Figure 5) except for Tyr62, which is hydrogen bonded to a bridging water molecule.

Interestingly, an additional electron density at the active site region appeared in the final stages of refinement and was fitted as a phosphate ion (shown as red spheres in Figure 5). The rationale for fitting this density as a phosphate ion is based on the geometry of the density and because the phosphate ion was used in the crystallization solution. ACTIBIND was crystallized as reported previously using 20% PEG 3350 and 0.2 M ammonium dihydrogen phosphate. Indeed, we found that the oxygen atoms of the phosphate ion are involved in hydrogen bonding to the three His residues at the active site (His115 (Nε2, 2.71 Å), His110 (Nε2, 2.51 Å), His51 (Nε23.1 Å)) and to Trp54 (Nε1 3.3 Å) residue at the binding site). In the RNase Rh crystal structure, the phosphate binding site is occupied by a water molecule.

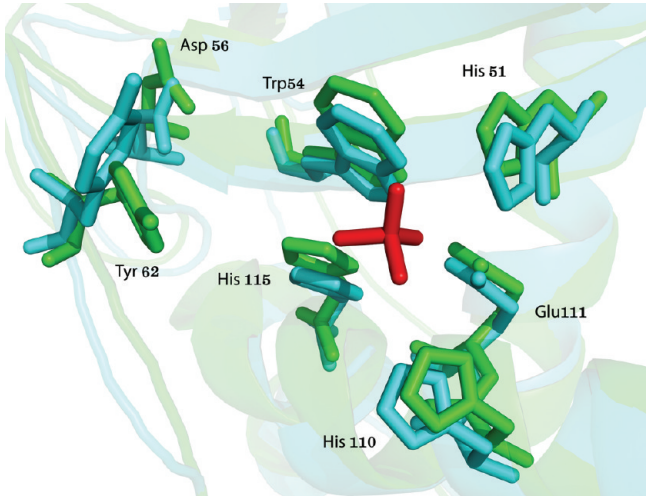

Figure 5. Superposition of the active site residues of ACTIBIND (in green) and RNase Rh (in blue). His51, His110, His115, and Trp54 (ACTIBIND numbering) are hydrogen bonded to the phosphate ion (shown in red) at the active site.

An additional electron density at the active site region was initially modeled as an AMP molecule (or a GMP one) similar to that which had previously been found in the crystal structure of T2 RNase from *E. coli*. However, this proved to be unsuccessful because the phosphate ion had shifted. We also tried to model a 5-deoxy-β-L-xylofuranosyl-pyrimidine molecule with an occupancy of 0.5 with the pyrimidine base hydrogen bonded to Asp97 (2.54 Å) main chain (2.96 Å) and to Asp37 (3.4 Å). However, the molecule refined to a distorted stereochemical conformation and the density was left unmodeled. It is possible that the electron density at the active site region corresponds to a disordered nucleotide.

The Glycosylation Sites. On the basis of the NetNGly 1.0 server, ACTIBIND was predicted to have two N-glycosylation sites at Asn74 and at Asn83. These residues are located on the surface of the molecule at the opposite ends of a short α-helix composed of residues 75−83 and are at a distance of 14 Å from each other (Figure 6). Both asparagine residues are part of an Asn-Xaa-Ser/Thr motif which is typical for N-glycosylation site. In the final stages of refinement, the extra electron density next to these two residues was assigned as *N*-acetyl-glucose amine (NAG) molecules. Two NAG molecules were fitted to the electron density next to Asn74, and only one NAG molecule was fitted next to Asn83. No additional electron density was found next to the NAG molecules bound to Asn83.

It was previously argued that the RNase T2 family shows a wide variation in carbohydrate content between the different taxa.[1] Irie et al. found in *Aspargillus saitoi* RNase M, which is a

dx.doi.org/10.1021/jm1015507 | J. Med. Chem. 2012, 55, 1013−1020

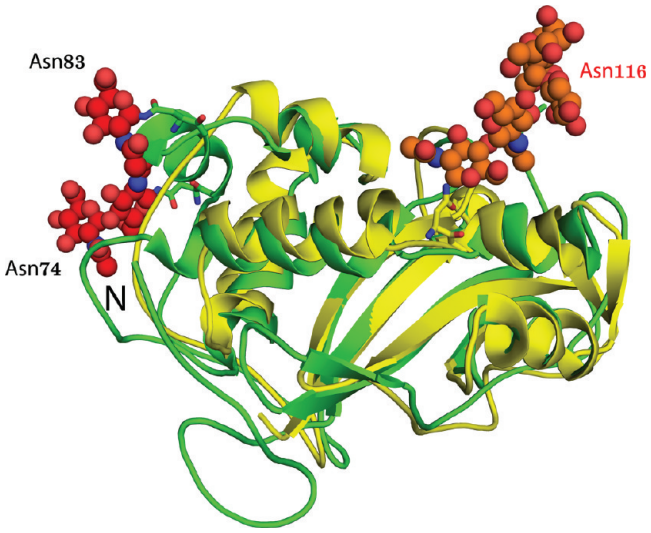

Figure 6. Glycosylation sites of ACTIBIND and S_3 RNase (PDB entry 1iqq). ACTIBIND is shown as a green ribbon and S_3 RNase as a yellow ribbon. NAG molecules at the glycosylation sites of ACTIBIND (Asn74 and Asn83) are shown as sphere and glycosylation sites of S_3 RNase (Asn116) as an orange sphere.

close homologue of ACTIBIND, about 14 residues of mannose, one or two of glucose, and three of glucosamines.[30] On the other hand, Uchida[31] reported that RNase T2 contains mannose and glucose but not amino sugars. It is clear that the degree of glycosylation of ACTIBIND includes additional sugar molecules as also indicated by the MALDI-TOF-MS study, but no electron density was found next to the refined NAG molecules.

DISCUSSION

In the present study, we have characterized, crystallized, and determined the three-dimensional structure of ACTIBIND. We compared the crystal structure and the biological activity of ACTIBIND with other T2 RNases in order to identify the structural motifs involved in its biological activity as an antitumorigenic agent. Our biochemical characterization indicated that ACTIBIND is a thermostable T2 RNase with a T_m of 55.9 °C, which is similar to other members of the T2 RNase family. For example, T2 RNase of *Aspergillus oryzae* has a T_m of 55.3 °C, for which reason it was suggested that the stability of the native state is predominantly due to the slow rate of unfolding.[32] Kimura et al.[27] reported that RNase MC1 thermostability as well as that of other T2 RNases is achieved by conserved amino acid residues at the C-terminal region. They concluded that these residues are responsible for the α-helix bundle and β-sheet structures and may be a prerequisite constraint in the evolution of the T2 RNase family. Sequence and structural comparison of ACTIBIND and RNase MC1 revealed similarities in the C-terminal region. The conserved residues include Phe140, Pro153, and Val 205 that are identical in both RNases. Also residues Phe139, Val143, Ala156, Tyr202, and Tyr231 (ACTIBIND numbering) are similar (see Figure 7), suggesting that that the conserved region at the C-terminal region contributes to ACTIBIND thermostability.

Because the anticarcinogenic and antiangiogenic activity of ACTIBIND was found to be common to several other T2 RNases (Figure 3), we performed structural alignments of ACTIBIND with RNase Rh, RNase MC1, RNase LE, S_3 RNase, S_{F11} RNase, and RNase I. The results indicated a considerable similarity of the overall crystal structures (Figure 8). The molecular core of these RNases is almost identical, whereas the

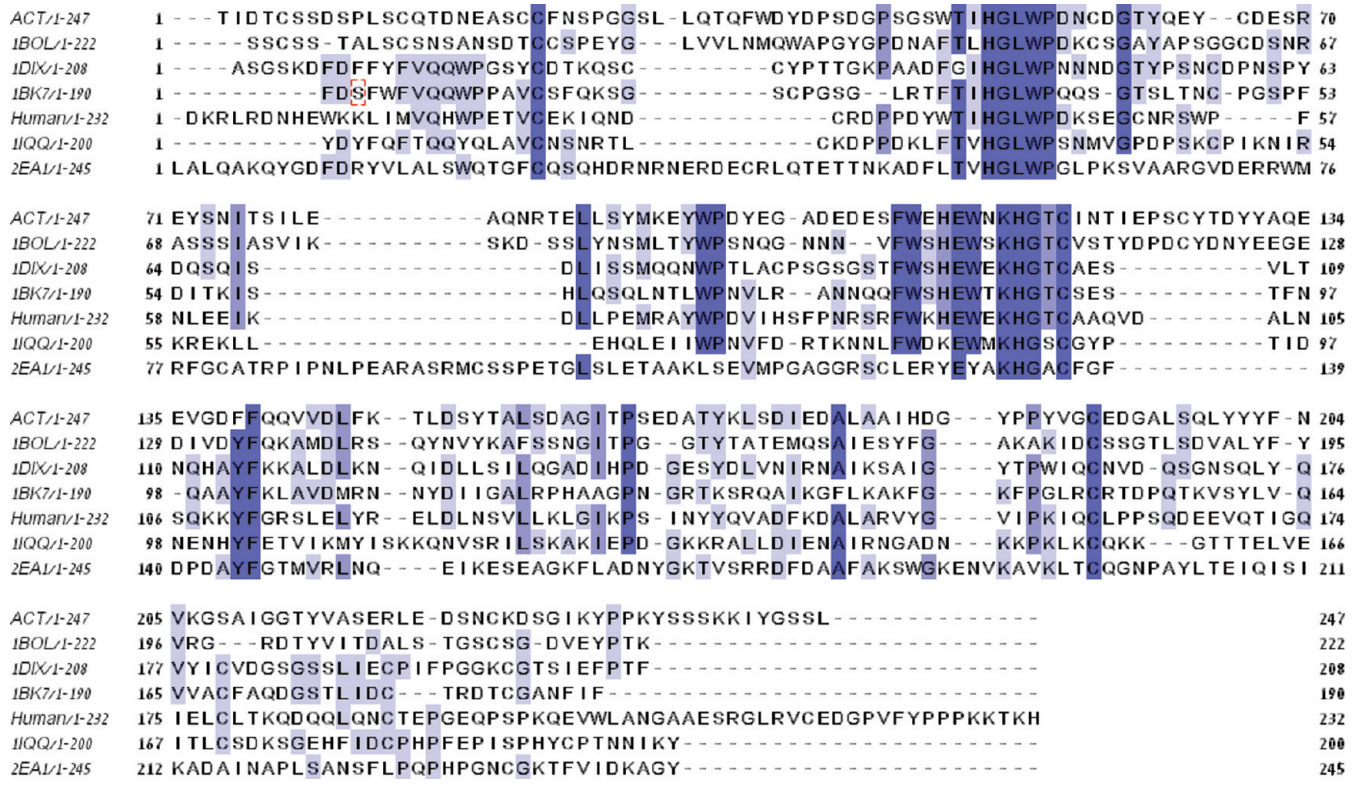

Figure 7. Sequence alignment of ACTIBIND (ACT PDB entry 3tbz) and RNase Rh (PDB entry 1bol), RNase LE (PDB entry 1dix), RNase MC1 (PDB entry 1bk7), human RNASET2, S_3 RNase (PDB entry 1iqq) and *E. coli* RNase I (PDB entry 2ea1).

dx.doi.org/10.1021/jm1015507 | *J. Med. Chem.* 2012, 55, 1013–1020

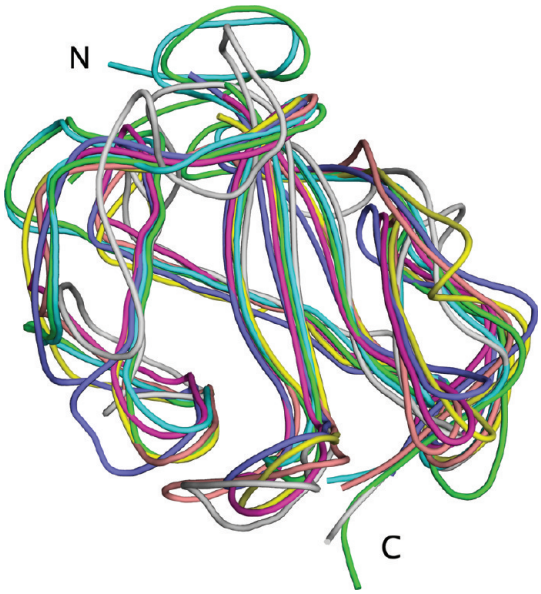

Figure 8. Superposition of the crystal structures of ACTIBIND (green) and RNase Rh (PDB entry 1bol, cyan), *E. coli* RNase I (PDB entry 2ea1, gray), RNase LE (PDB entry 1dix, pink), RNase MC1 (PDB entry 1bk7, magenta), S_3 RNase (PDB entry 1iqq, yellow), and S_{F11} RNase (PDB entry 1ioo, dark-blue).

differences are found in the outer loops at the surface of the molecules. Therefore, we have a reason to believe that the mutual ability of several T2 RNases to bind actin as well as to inhibit angiogenesis is located at a similar molecular core.

Previously, it was suggested that the glycosylation sites of T2 RNases, which are located on the surface of the molecules, are involved in their anticarcinogenic activity. Superposition of the crystal structures of ACTIBIND and S_3 RNase showed a high similarity in the three-dimensional protein structure but considerable differences in location and orientation of the glycan side chains (Figure 6). Our preliminary results showed that deglycosylated ACTIBIND retains its anticarcinogenic activity (data not shown). Both findings suggest that neither the glycan sites themselves nor their location on the molecule can be considered as part of the pharmacophor of T2 RNases as antitumorigenic or antiangiogenic agents. This further supports the claim[33,34] that glycans play a role in maintaining glycoprotein stability and in improving their solubility rather than their biological activity.

We used the 1.8 Å crystal structure determined here to elucidate the sites that are important for ACTIBIND's antitumorigenic activity. To accomplish this, we performed sequence (Figure 7) and structural alignment of ACTIBIND with several T2 RNases including RNase I from *E. coli* and human RNASET2 (Figure 8). The sequence alignments revealed that the most conserved region is the RNA degrading active site: residues 51−55 (ACTIBIND numbering)-HGLWP and residues 111−116 (ACTIBIND numbering)-EWXKHG. In addition to these conserved regions, several conserved amino acids were identified: Cys22, Cys118, Phe140, and Cys191.

Structural alignments were used to identify the molecular location of these conserved region on the three-dimensional structures of members of the T2 RNase family. In particular, we examined whether this conserved region and amino acids are located on the surface of the molecules. We found that Phe140 is part of the core of the molecule, while the other conserved residues or regions are found on the surface. These include the two cysteine residues (Cys22 and Cys191) which are conserved among the entire T2 RNase family and are located on the surface of the molecule. Interestingly, each of these cysteine residues is found at a distance of about 20 Å apart from the active site.

CONCLUSION

In summary, we suggest a model in which two structural motifs are involved in the binding of T2 RNases to actin. Each of the motifs is composed of part of the conserved active site and one conserved surface cysteine residue. One motif is composed of residue Cys22 and the conserved region of residues 51−55, which were found about 20 Å apart. The other motif is composed of Cys191 and the conserved region of residues 111−116, which are also about 20 Å apart. The suggested structural motifs are in agreement with our previous report[9] in which we showed that ACTIBIND has two actin binding sites. Efforts to purify new variants of ACTIBIND in which the relevant amino acids are replaced or deletion mutants are in progress.

EXPERIMENTAL SECTION

Protein Purification. ACTIBIND or *Aspergillus niger* B1 (CMI CC 324626) T2 RNase was purified as described previously.[8] The purification included growing *Aspergillus niger* B1 on liquid culture containing 1% (w/v) wheat flour and 0.05% (w/v) $(NH_4)_2SO_4$, dialysis, and separation onto a Fractogel EMD-TMAE 650 (M) 26/10 (Merck, Darmstadt, Germany) column, which was equilibrated with 20 mM sodium acetate at pH 6, and elution using NaCl.

Protein Analysis. Differential scanning calorimetry (DSC) measurements were performed using 0.75 mg/mL protein dissolved in a 0.1 M sodium phosphate and 0.5 M glycerol buffer (pH 7.4). The scan rate was 1.0 °C/min from 10 to 115 °C on a VP-Capillary DSC platform (MicroCal, LLC, Northampton, MA). The DSC profile was calculated using the Origin 7.0 software. MALDI-TOF analysis was performed using the Applied Biosystems 4700 MALDI TOF. SDS-PAGE (12.5% Tricine) was performed according to Laemmli[35] and stained with Coomassie blue.

Activity Gel. Crystals of ACTIBIND were washed quickly with water and dissolved in 20 μL of distilled water. Activity gel was performed as modified from Roiz and Shoseyov.[36] An SDS gel containing ACTIBIND was renatured by washing twice for 15 min each with 20 mM sodium acetate pH 4.5 containing 25% (v/v) isopropyl alcohol and then twice for 15 min each with buffer alone. The renatured gel was laid over a plate containing 0.1% RNA and 0.8% agarose in 20 mM sodium acetate and incubated at 37 °C for 30 min. The gel was then removed, and the agarose plate was stained with 0.02% (w/v) toluidine blue in the buffer to visualize RNase activity.

Human Umbilical Vein Endothelial Cell (HUVEC) Angiogenesis Assay. As previously described,[10] freshly isolated human umbilical vein endothelial cells (HUVEC) were maintained in M199 medium supplemented with 20% fetal calf serum (FCS), 1% glutamine, 1% antibiotic−antimycotic solution, 0.02% endothelial cell growth factor (ECGF), and 50 units heparin in 10 mL medium. They were then plated in a 96-well plate (14000 cells/well) previously coated with growth factor-depleted Matrigel in 120 μL of M199 medium containing 5% FCS and supplemented with angiogenin or basic fibroblast growth factor (bFGF; 1 μg/mL each). Different T2-RNases were added to a final concentration of 10 μM each. Phosphate-buffered saline (PBS) was used as control. After overnight incubation at 37 °C, the plates were photographed and the extent of tube formation was assessed (N = 5).

Crystallization. Crystallization experiments were set up using the hanging-drop vapor-diffusion method with siliconized coverslips and Linbro 24-well tissue culture plates. In these experiments, droplets ranging in size from 5 to 10 μL were prepared by mixing an equal

volume of protein solution and reservoir solution, and they were equilibrated with 1.0 mL of reservoir solution at room temperature (293 K). The protein solution was prepared by dissolving 17 mg of lyophilized and purified ACTIBIND in 0.5 mL of distilled water.[9] Crystals suitable for data collection were achieved by using the Ion/PEG screen of Hampton Research (condition 43 of Ion/PEG screen), which contains 20% PEG 3350 and 0.2 M ammonium dihydrogen phosphate. One to four crystals appeared within the droplet after three days and grew to their maximal size of $0.5 \times 0.5 \times 0.5$ mm^3 within one week.

High Resolution Data Collection. Crystals were transferred from the mother liquor to the cryoprotectant (12% glycerol and 87% mother liquor) then were scooped up in a cryo-loop and exposed to a cold nitrogen stream (Oxford Instruments), where they were rapidly frozen. About 50 crystals were screened prior to the data collection using the SAM screening system.[37] Diffraction patterns for each crystal were analyzed and scored using Web-Ice.[38] The three best crystals were selected for full data collection on the Stanford Synchrotron Radiation Light source (SSRL) wiggler beamline (BL7−1), at wavelength of 0.98 Å and a Q315r CCD detector. The data from the crystals diffracting to highest resolution were scaled and merged using SCALA, and the intensities were converted to amplitudes using TRUNCATE.[39,40] The crystals belonged to the space group $P3_221$. The point symmetry was determined by using LABELIT program,[41] and the correct enantiomorph was determined by trial and error during phasing.

Structure Determination and Refinement. The structure of ACTIBIND was solved by the molecular replacement method with the MOLREP program[42] using the data to 2.5 Å resolution and the crystal structure of RNase Rh as the starting model. The initial polyalanine model was modified and rebuilt using ARPwARP[43,44] program. The model was refined with REFMAC[45] and additional waters added with the ARPwARP. Building of ligands and disordered areas in the electron density was done with the graphics program COOT.[46]

■ ASSOCIATED CONTENT

Accession Codes

Coordinates and structure factors have been deposited in the Protein Data Bank with accession number 3tbz.

■ AUTHOR INFORMATION

Corresponding Author

*Phone: 972-8-647-9930. Fax: 972-8-647-9931. E-mail: almogo@bgu.ac.il.

■ ACKNOWLEDGMENTS

We gratefully thank Dr. Ofra Lotan for her most valuable contribution to the preparation of this manuscript.

■ ABBREVIATIONS USED

RNases, ribonucleases; DSC, differential scanning calorimetry; DMH, dimethylhydrazine; HUVEC, human umbilical vein endothelial cell; FCS, fetal calf serum; ECGF, endothelial cell growth factor; NAG, *N*-acetyl-D-glucosamine; MALDI-TOF-MS, matrix assisted laser desorption ionization time-of-flight mass spectrometry; bFGF, basic fibroblast growth factor

■ REFERENCES

(1) Deshpande, R. A.; Shankar, V. Ribonucleases from T2 family. *Crit. Rev. Microbiol.* **2002**, *28* (2), 79−122.

(2) Luhtala, N.; Parker, R. T2 Family ribonucleases: ancient enzymes with diverse roles. *Trends Biochem. Sci.* **2010**, *35*, 253−259.

(3) Irie, M.; Ohgi, K. Ribonuclease T2. *Methods Enzymol.* **2001**, *341*, 42−55.

(4) Nurnberger, T.; Abel, S.; Jost, W.; Glund, K. Induction of extracellular ribonucleases in cultured tomato cells upon phosphate starvation. *Plant Physiol.* **1990**, *92*, 970−976.

(5) Clarke, A. E.; Newbigin, E. Molecular aspects of self-incompatibility in flowering plants. *Annu. Rev. Genet.* **1993**, *27*, 257−279.

(6) Silva, N. F.; Goring, D. R. Mechanisms of self-incompatibility in flowering plants. *Cell. Mol. Life Sci.* **1997**, *58*, 1988−2007.

(7) Lers, A.; Khalchitski, A.; Lomaniec, E.; Burd, S.; Green, P. J. Senescence-induced RNases in tomato. *Plant Mol. Biol.* **1998**, *36* (3), 439−449.

(8) Roiz, L.; Ozeri, U.; Goren, R.; Shoseyov, O. Characterization *Aspergillus niger* B-l RNase and its inhibitory effect on pollen germination and pollen tube growth in selected tree fruit. *J. Am. Soc. Hort. Sci.* **2000**, *125* (1), 9−14.

(9) de Leeuw, M.; Roiz, L.; Smirnoff, P.; Schwartz, B.; Shoseyov, O.; Almog, O. Binding assay and preliminary X-ray crystallographic analysis of ACTIBIND, a protein with anticarcinogenic and antiangiogenic activities. *Acta Crystallogr., Sect. F: Struct. Biol. Cryst. Commun.* **2007**, *63* (Pt 8), 716−719.

(10) Roiz, L.; Smirnoff, P.; Bar-Eli, M.; Schwartz, B.; Shoseyov, O. ACTIBIND, an actin-binding fungal T2-RNase with antiangiogenic and anticarcinogenic characteristics. *Cancer* **2006**, *106* (10), 2295−2308.

(11) Hu, G. F.; Strydom, D. J.; Fett, J. W.; Riordan, J. F.; Vallee, B. L. Actin is a binding protein for angiogenin. *Proc. Natl. Acad. Sci. U.S.A* **1993**, *90* (4), 1217−1221.

(12) Schwartz, B.; Shoseyov, O.; Melnikova, V. O.; McCarty, M.; Leslie, M.; Roiz, L.; Smirnoff, P.; Hu, G. F.; Lev, D.; Bar-Eli, M. ACTIBIND, a T2 RNase, competes with angiogenin and inhibits human melanoma growth, angiogenesis, and metastasis. *Cancer Res.* **2007**, *67* (11), 5258−5266.

(13) Acquati, F.; Nucci, C.; Bianchi, M. G.; Gorletta, T.; Taramelli, R. Molecular cloning, tissue distribution, and chromosomal localization of the human homolog of the R2/Th/Stylar ribonuclease gene family. *Methods Mol. Biol.* **2001**, *160*, 87−101.

(14) Trubia, M.; Sessa, L.; Taramelli, R. Mammalian Rh/T2/S-glycoprotein ribonuclease family genes: cloning of a human member located in a region of chromosome 6 (6q27) frequently deleted in human malignancies. *Genomics* **1997**, *42* (2), 342−344.

(15) Cooke, I. E.; Shelling, A. N.; Le Meuth, V. G.; Charnock, M. L.; Ganesan, T. S. Allele loss on chromosome arm 6q and fine mapping of the region at 6q27 in epithelial ovarian cancer. *Genes, Chromosomes Cancer* **1996**, *15* (4), 223−233.

(16) Saito, S.; Saito, H.; Koi, S.; Sagae, S.; Kudo, R.; Saito, J.; Noda, K.; Nakamura, Y. Fine-scale deletion mapping of the distal long arm of chromosome 6 in 70 human ovarian cancers. *Cancer Res.* **1992**, *52* (20), 5815−5817.

(17) Theile, M.; Seitz, S.; Arnold, W.; Jandrig, B.; Frege, R.; Schlag, P. M.; Haensch, W.; Guski, H.; Winzer, K. J.; Barrett, J. C.; Scherneck, S. A defined chromosome 6q fragment (at D6S310) harbors a putative tumor suppressor gene for breast cancer. *Oncogene* **1996**, *13* (4), 677−685.

(18) Tibiletti, M. G.; Sessa, F.; Bernasconi, B.; Cerutti, R.; Broggi, B.; Furlan, D.; Acquati, F.; Bianchi, M.; Russo, A.; Capella, C.; Taramelli, R. A large 6q deletion is a common cytogenetic alteration in fibroadenomas, pre-malignant lesions, and carcinomas of the breast. *Clin. Cancer Res.* **2000**, *6* (4), 1422−1431.

(19) Honchel, R.; McDonnell, S.; Schaid, D. J.; Thibodeau, S. N. Tumor necrosis factor-alpha allelic frequency and chromosome 6 allelic imbalance in patients with colorectal cancer. *Cancer Res.* **1996**, *56* (1), 145−149.

(20) Kurihara, H.; Mitsui, Y.; Ohgi, K.; Irie, M.; Mizuno, H.; Nakamura, K. T. Crystal and molecular structure of RNase Rh, a new class of microbial ribonuclease from *Rhizopus niveus*. *FEBS Lett.* **1992**, *306* (2−3), 189−192.

(21) Kurihara, H.; Nonaka, T.; Mitsui, Y.; Ohgi, K.; Irie, M.; Nakamura, K. T. The crystal structure of ribonuclease Rh from

Rhizopus niveus at 2.0 A resolution. *J. Mol. Biol.* **1996**, *255* (2), 310−320.
(22) Tanaka, N.; Arai, J.; Inokuchi, N.; Koyama, T.; Ohgi, K.; Irie, M.; Nakamura, K. T. Crystal structure of a plant ribonuclease, RNase LE. *J. Mol. Biol.* **2000**, *298* (5), 859−873.
(23) Nakagawa, A.; Tanaka, I.; Sakai, R.; Nakashima, T.; Funatsu, G.; Kimura, M. Crystal structure of a ribonuclease from the seeds of bitter gourd (*Momordica charantia*) at 1.75 A resolution. *Biochim. Biophys. Acta* **1999**, *1433* (1−2), 253−260.
(24) Matsuura, T.; Sakai, H.; Unno, M.; Ida, K.; Sato, M.; Sakiyama, F.; Norioka, S. Crystal structure at 1.5Å resolution of *Pyrus pyrifolia* pistil ribonuclease responsible for gametophytic self-incompatibility. *J. Biol. Chem.* **2001**, *276* (48), 45261−45269.
(25) Ida, K.; Norioka, S.; Yamamoto, M.; Kumasaka, T.; Yamashita, E.; Newbigin, E.; Clarke, A. E.; Sakiyama, F.; Sato, M. The 1.55 A resolution structure of *Nicotiana alata* S(F11)-RNase associated with gametophytic self-incompatibility. *J. Mol. Biol.* **2001**, *314* (1), 103−112.
(26) Zhu, L. Q.; Gangopadhyay, T.; Padmanabha, K. P.; Deutscher, M. P. *Escherichia coli* rna gene encoding RNase I: cloning, overexpression, subcellular distribution of the enzyme, and use of an rna deletion to identify additional RNases. *J. Bacteriol.* **1990**, *172* (6), 3146−3151.
(27) Kimura, K.; Numata, T.; Kakuta, Y.; Kimura, M. Amino acids conserved at the C-terminal half of the ribonuclease T2 family contribute to protein stability of the enzymes. *Biosci., Biotechnol., Biochem.* **2004**, *68* (8), 1748−1757.
(28) Laskowski, R. A.; Macarthur, M. W.; Moss, D. S.; Thornton, J. M. Procheck—A Program to Check the Stereochemical Quality of Protein Structures. *J. Appl. Crystallogr.* **1993**, *26*, 283−291.
(29) Levitt, M.; Chothia, C. Structural patterns in globular proteins. *Nature* **1976**, *261* (5561), 552−558.
(30) Irie, M.; Harada, M.; Negi, T.; Samejima, T. Some chemical and physical properties of ribonuclease from *Aspergillus saitoi*. *J. Biochem.* **1971**, *69* (5), 881−892.
(31) Uchida, T. Purification and properties of RNase T2. *J. Biochem.* **1966**, *60* (2), 115−132.
(32) Kawata, Y.; Hamaguchi, K. Stability of ribonuclease T2 from *Aspergillus oryzae*. *Protein Sci.* **1995**, *4* (3), 416−420.
(33) Parry, S.; Newbigin, E.; Craik, D.; Nakamura, K. T.; Bacic, A.; Oxley, D. Structural analysis and molecular model of a self-incompatibility RNase from wild tomato. *Plant Physiol.* **1998**, *116* (2), 463−469.
(34) Rademacher, T. W.; Parekh, R. B.; Dwek, R. A. Glycobiology. *Annu. Rev. Biochem.* **1988**, *57*, 785−838.
(35) Laemmli, U. K. Cleavage of structural proteins during the assembly of the head of bacteriophage T4. *Nature* **1970**, *227* (5259), 680−685.
(36) Roiz, L.; Shoseyov, O. Stigmatic RNase in self-compatible peach (*Prunus persica*). *Int J Plant Sci.* **1995**, *156*, 37−41.
(37) Cohen, A. E.; Ellis, P. J.; Miller, M. D.; Deacon, A. M.; Phizackerley, R. P. An automated system to mount cryo-cooled protein crystals on a synchrotron beamline, using compact sample cassettes and a small-scale robot. *J. Appl. Crystallogr.* **2002**, *35*, 720−726.
(38) Gonzalez, A.; Moorhead, P.; McPhillips, S. E.; Song, J.; Sharp, K.; Taylor, J. R.; Adams, P. D.; Sauter, N. K.; Soltis, S. M. Web-Ice: integrated data collection and analysis for macromolecular crystallography. *J. Appl. Crystallogr.* **2008**, *41*, 176−184.
(39) CCP4, Coolaborative Computation Project 4. *Acta Crystallogr., Sect. D: Biol. Crystallogr.* **1994**, *50*, 760−763.
(40) Evans, P. R. Some notes on choices in data collection. *Acta Crystallogr., Sect. D: Biol. Crystallogr.* **1999**, *55*, 1771−1772.
(41) Sauter, N. K.; Grosse-Kunstleve, R. W.; Adams, P. D. Robust indexing for automatic data collection. *J. Appl. Crystallogr.* **2004**, *37*, 399−409.
(42) Vagin, A.; Teplyakov, A. MOLREP: an automated program for molecular replacement. *J. Appl. Crystallogr.* **1997**, *30*, 1022−1025.
(43) Lamzin, V. S.; Wilson, K. S. Automated refinement for protein crystallography. *Methods Enzymol.* **1997**, *277*, 269−305.
(44) Perrakis, A.; Sixma, T. K.; Wilson, K. S.; Lamzin, V. S. wARP: improvement and extension of crystallographic phases by weighted averaging of multiple-refined dummy atomic models. *Acta Crystallogr., Sect. D: Biol. Crystallogr.* **1997**, *53* (Pt 4), 448−455.
(45) Vagin, A. A.; Steiner, R. A.; Lebedev, A. A.; Potterton, L.; McNicholas, S.; Long, F.; Murshudov, G. N. REFMAC5 dictionary: organization of prior chemical knowledge and guidelines for its use. *Acta Crystallogr., Sect. D: Biol. Crystallogr.* **2004**, *60* (Pt12 Pt 1), 2184−2195.
(46) Emsley, P.; Cowtan, K. Coot: model-building tools for molecular graphics. *Acta Crystallogr., Sect. D: Biol. Crystallogr.* **2004**, *60* (Pt 12 Pt 1), 2126−2132.